ARTICLES
PUBLISHED ONLINE: 5 AUGUST 2012 | DOI: 10.1038/NPHYS2384
nature physics

Local thermometry of neutral modes on the quantum Hall edge

Vivek Venkatachalam[1†], Sean Hart[1†], Loren Pfeiffer[2], Ken West[2] and Amir Yacoby[1*]

Electrons in two dimensions and strong magnetic fields can form an insulating two-dimensional system with conducting one-dimensional channels along the edge. Electron interactions in these edges can lead to independent transport of charge and heat, even in opposite directions. Here, we heat the outer edge of such a quantum Hall system using a quantum point contact. By placing quantum dots upstream and downstream from the heater, we measure both the chemical potential and temperature of that edge to study charge and heat transport, respectively. We find that charge is transported exclusively downstream, but heat can be transported upstream when the edge has additional structure related to fractional quantum Hall (FQH) physics. Surprisingly, this can occur even when the bulk is in an integer quantum Hall state and the edge contains no signatures of FQH charge transport. We also find an unexpected bulk contribution to heat transport at $\nu = 1$.

When a two-dimensional electron system (2DES) is subject to a strong perpendicular magnetic field and tuned such that the ratio of electrons to magnetic flux quanta in the system (ν) is near certain integer or fractional values, the bulk of the system develops a gap due to either quantization of kinetic energy (the integer quantum Hall, or IQH, effect) or strong correlations arising from non-perturbative Coulomb interactions (the FQH effect)[1]. Whereas the bulk (two-dimensional; 2D) is gapped and incompressible, the edge (1D) of the system contains compressible regions with gapless excitations that carry charge chirally around the system, in a direction determined by the external magnetic field. Compressible edge states have gained more attention recently owing to their ability to serve as a bus for quasiparticles that exist in exotic FQH phases[2,3]. These edges, however, can have considerable internal structure that is not apparent from bulk transport measurements.

The spatial structure of edges is dictated by the interplay between the external confining potential that defines the edge, a further harmonic confinement from the magnetic field, and Coulomb interactions. It was predicted[4] and verified[5–7] that for a smooth, topgate-defined confining potential, it is energetically favourable for the electron density to redistribute slightly to create alternating compressible and incompressible strips. This has the effect of spatially separating edges corresponding to transitions between different filling factors. Such an effect is not expected in sharper edges[8].

Perhaps more surprising than this spatial structure is the possibility of modes that carry energy (or heat) upstream, even as the magnetic field carries the injected charge downstream. The edge of the $\nu = 2/3$ FQH state was originally predicted to consist of a $\nu = 1$ edge of electrons travelling downstream with a $\nu = 1/3$ edge of holes propagating upstream[9,10]. This edge structure would suggest a two-terminal conductance of $G_{2T} = (4/3)(e^2/h)$. Scattering between the edges would lead to non-universal values in the range of $(2/3)(e^2/h) \leq G_{2T} \leq (4/3)(e^2/h)$. Experimentally, however, no such two-terminal conductance has been measured. Direct approaches to look for upstream charge transport in the time domain have similarly found no evidence[11]. This motivated a picture in which disorder induces scattering and equilibration between the edges, forcing the charge to travel exclusively downstream. Heat, however, would be allowed to travel diffusively upstream and downstream, leading to a non-zero thermal Hall conductivity and partial upstream heat transport at $\nu = 2/3$ (refs 12,13).

Evidence for upstream heat transport in a $\nu = 2/3$ edge was recently obtained by performing modified shot noise measurements[14]. Our approach studies the same state by directly placing thermometers upstream and downstream of a current-source heater to observe charge and heat transport along the edge. We will focus on low-energy transport properties, in contrast to another recent measurement with high degrees of charge imbalance along the edge[15].

As our heater, we use a lithographically fabricated quantum point contact (QPC), tuned to the tunnelling regime (Fig. 1c). Tunnelling of electrons through this QPC at elevated energy locally excites the outermost compressible component of a gate-defined edge[16]. This edge, in general, may have many spatially separated compressible components (dark grey regions in Fig. 1a). We then place quantum dots 20 μm upstream and downstream of the QPC to measure charge and heat transport (blue and red gates in Fig. 1a). The edge itself is defined by a separate pair of gates (green in Fig. 1a), and the perpendicular magnetic field defines a clockwise charge-propagation direction (with respect to Fig. 1). All measurements were carried out in a dilution refrigerator with a minimum electron temperature of 20 mK, measured with Coulomb blockade thermometry.

Charge signatures of edge reconstruction

To first characterize the structure of the edge that we are tunnelling charge into, we energize a subset of gates upstream (blue) and downstream (red) of the central QPC to create two more point contacts that serve as imperfect voltage probes ($R \sim 100\,\mathrm{k\Omega}$). This ensures that we measure the chemical potential of the outermost edge component alone[16]. Current is injected through the central QPC (10 pA sourced through O3 and drained at O6). The upstream chemical potential, $V1$–$V7$, was observed to be immeasurably small in all measurements, indicating that no charge is transported

[1]Department of Physics, Harvard University, Cambridge, Massachusetts 02138, USA, [2]Department of Electrical Engineering, Princeton University, Princeton, New Jersey 08544, USA. †These authors contributed equally to this work. *e-mail: yacoby@physics.harvard.edu.

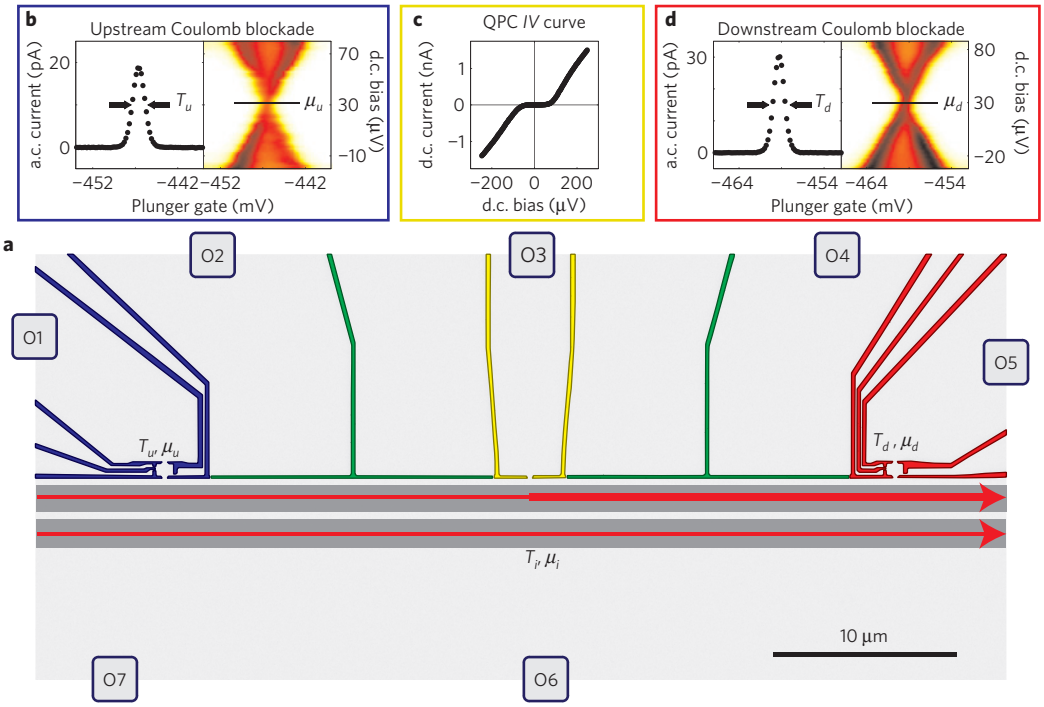

Figure 1 | Measurement overview. a, Scanning electron micrograph with coloured gates. O1–7 denote ohmic contacts. Injection of current through the central QPC (yellow) populates and heats the outermost quantum Hall edge channel. Deflector gates (green) adjacent to the injection site define the edge or can be de-energized to direct edge channels to floating ohmic contacts (O2 and O4). A quantum dot (red) located 20 μm downstream of the injection site is used to measure the temperature T_d and chemical potential μ_d of the outer edge channel. Similarly, an upstream dot (blue) measures T_u and μ_u. Inner edges may be present at a different temperature (T_i) and chemical potential (μ_i). Our measurements cannot determine edge widths, but there is some evidence that edge reconstruction may occur over several micrometres in these devices (see Supplementary Fig. S12). **b**,**d**, Coulomb blockade peaks and diamonds for the quantum dots. The temperature is determined from the Coulomb blockade peak width. The chemical potential is determined by zeroing the voltage bias across the quantum dot. **c**, The *IV* characteristic of the QPC. For charge transport (Fig. 2), the QPC was biased just beyond blockade. Heat transport measurements (Fig. 3) were taken at all points of the *IV* curve.

upstream on a 20 μm scale. The downstream chemical potential, $V5$–$V7$, can be used to determine the resistance of the edge connecting the source to the probe (the local Hall resistance R_L). This resistance is plotted in blue in Fig. 2. Further measurement details can be found in Supplementary Information SA.

For magnetic fields (B) between 2 and 8 T, the measured value $R_L = 1(h/e^2)$ indicates that the charge is carried between the injector and detector by electronic modes that behave similarly to an IQH $\nu = 1$ edge. Inner edges can (and must, at fields below 6 T) be present, as can be seen by comparing R_{xy} with R_L. These inner edges, however, do not carry any of the injected charge. Above 8 T, we find that R_L is quantized to $R_L = (3/2)(h/e^2)$ even though the bulk is at $\nu = 1$ (ref. 17). This suggests that the edge has additional structure consisting of alternating compressible and incompressible regions that are spatially separated, as indicated in Fig. 2IV. In this situation, we access only the outermost edge of the incompressible $\nu = 2/3$ strip located outside the $\nu = 1$ bulk. The robust quantization that we observe indicates that no charge leaks out of this outermost $\nu = 2/3$ edge over the 20 μm separating the injector from the detector.

The edge-deflecting gates (green in Fig. 1a) can be de-energized to deflect the edges into floating ohmic contacts located 250 μm away (O2 and O4), where they will chemically equilibrate and thermally cool (although some equilibration and cooling may occur before the edges reach the ohmic contacts). If we repeat this charge transport measurement with the deflector gates de-energized, we continue to monitor no upstream charge transport. However, the downstream resistance is observed to match exactly the bulk value of R_{xy}, plotted in black in Fig. 2. This indicates that our deflection process does, indeed, force all edges to fully equilibrate their chemical potentials in ohmic contacts O2 and O4, providing an important control for the heat transport measurements discussed below.

Heat transport at $\nu = 2$ and $\nu = 3$

To characterize heat transport, we energize all of the gates upstream and downstream of the central QPC to form quantum dots, which serve as thermometers to measure the temperature of the edge. This is similar to another recent spectroscopic approach[18–20]. The width of the Coulomb blockade peak as a function of gate voltage can be translated into the temperature of the leads (Fig. 1b, details in Supplementary Information SA).

With the thermometers active, we inject current through the QPC set to an average transmission of 15% to create a non-equilibrium population in the outermost edge (Fig. 1c). The low transmission ensures that we inject solely electrons into the edge (no FQH edges are fully transmitted). These energetic electrons, however, are not necessarily the elementary excitations of the edge and will therefore excite the natural edge modes as they decompose. By increasing the bias across the QPC, we vary the current (and therefore the power) being delivered to the edge. We monitor both the chemical potential and temperature of the edge at the upstream and downstream dots (Fig. 1b,d).

Measurements are first performed with the deflector gates energized, to measure heat transport associated with the edge (red and blue curves in rows 1 and 2 of Fig. 3). We then repeat the procedure with the deflector gates off, to measure any background heating not associated with the edge (cyan and magenta curves in rows 1 and 2 of Fig. 3). The difference between these two temperatures gives us a measure of the excess heat carried by the edge (bottom row in Fig. 3, red is downstream and blue is upstream temperature).

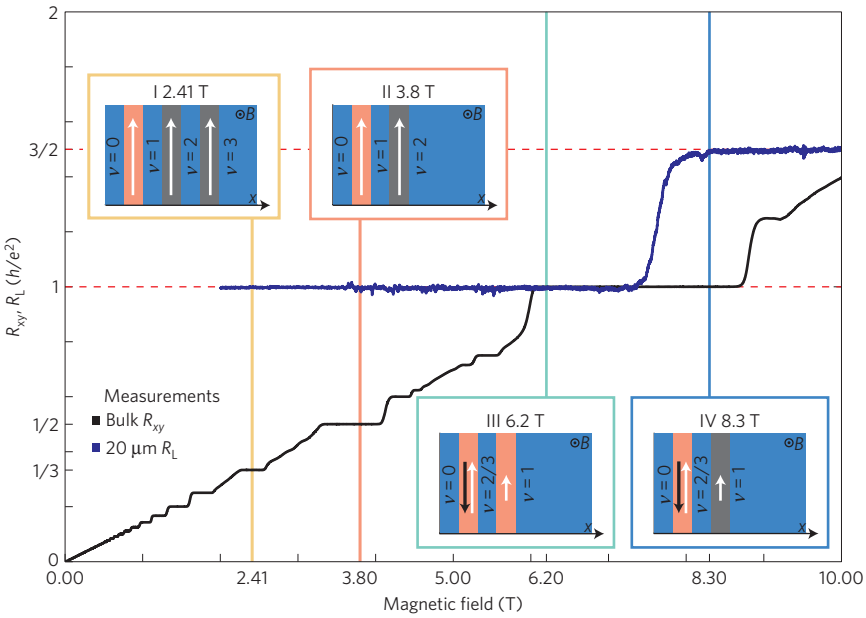

Figure 2 | Local charge transport. Plateaux in R_{xy} (black) indicate bulk quantum Hall states. Plateaux in R_L (blue) reveal the structure of the edge. The insets depict the qualitative structure of the sample edge at various magnetic fields, with incompressible regions shown in light blue and labelled by filling factor. In the intervening compressible channels, white arrows point in the direction of charge flow. The arrow length specifies a charge conductance of $G = 1$, 2/3 or 1/3 in units of e^2/h. Black arrows indicate neutral modes that carry energy upstream. The channels highlighted in red contribute to charge transport at the voltage probe. (I),(II), When the bulk filling factor is $\nu = 2$ or $\nu = 3$, the edge is composed of integer channels with the outermost channel having conductance $G = 1$. At the voltage probe, the excess current is carried solely by the outermost channel. (III),(IV), Outside the bulk $\nu = 1$ state the edge is reconstructed, resulting in an outermost $G = 2/3$ charge channel. The remaining 1/3 conductance can be found on a spatially separated inner edge located in the compressible region between the $\nu = 2/3$ and $\nu = 1$ incompressible regions. At 8.3 T, the excess current is carried to the voltage probe only by the outermost channel. At 6.2 T, the edge channels come to the same potential before reaching the voltage probe, resulting in $R_L = 1$. Dashed red lines indicate quantized values of R_L.

At the two lowest fields that were measured (2.41 and 3.8 T), our charge transport measurements indicate that we are injecting charge into a $\nu = 1$ edge situated outside an incompressible bulk at filling $\nu = 3$ or $\nu = 2$, respectively. This is depicted schematically in Fig. 2I,II and in Fig. 4II. By monitoring the chemical potential as we vary the injected power, we find that charge is carried exclusively by the outermost $\nu = 1$ edge over the entire range of measurement (Supplementary Information SA).

At 2.41 T, when the bulk is at $\nu = 3$, there is no measurable background heating either upstream or downstream. When the deflectors are turned on, we find heating downstream but none upstream. When the bulk is at $\nu = 2$, we find about 2–3 mK of background heating that is perfectly cancelled in the upstream direction. Thus, in both cases, we find that heat carried by edge modes is transported exclusively downstream. Although this strict downstream heat transport in the IQH regime is expected and matches previous measurements[14,21], surprisingly, the magnitude of the temperature observed does not agree with what one would expect from quantized thermal transport (assuming an equilibrated edge):

$$K_H \equiv \frac{\partial J_E}{\partial T} = n\frac{\pi^2}{3}\frac{k_B^2}{h}T \Rightarrow T = \frac{\sqrt{6hJ_E/n}}{\pi k_B}$$

where J_E is the power carried by the edge and n is the number of IQH edges participating in transport[13]. At $\nu = 2$, for an injected power of 350 fW, we expect an edge temperature between 430 and 608 mK, depending on how well the two edges thermally equilibrate ($n = 2$ or $n = 1$). Our measured temperature of 30 mK indicates that a substantial quantity of heat is transferred out of the edge[19]. We can model the behaviour of heat transport for out-of-equilibrium Fermi systems (Supplementary Information SB), which indicates a similar temperature deficiency. Both models, however, give the correct shape for the temperature versus power curves presented in Fig. 3.

Neutral modes associated with the $\nu = 2/3$ and $\nu = 1$ edges

At the highest measured field, 8.3 T, charge transport (Fig. 2) indicates that we have an incompressible $\nu = 2/3$ strip outside a $\nu = 1$ bulk, depicted schematically in Fig. 2IV. Here we see substantially more background heating, both upstream and downstream. This bulk heating at $\nu = 1$ is unexpected and has not previously been observed, although a similar result at $\nu = 4/3$ has recently been reported[22]. Further details can be found in Supplementary Information SC. After subtracting contributions from the bulk (deflectors energized), we still find an upstream temperature rise of 5 mK at 300 fW, compared with a downstream rise of 11 mK. Such upstream heating is consistent with the predicted upstream thermal conductivity of the outer $\nu = 2/3 \rightarrow 0$ edge[13], although the asymmetry between upstream and downstream temperatures suggests that the inner $\nu = 1 \rightarrow 2/3$ edge (which is expected to carry heat preferentially downstream) is partially participating in heat transport.

At the second highest measured field, 6.2 T, one would expect, on the basis of charge transport, behaviour similar to what we find when the bulk is at $\nu = 2$ or $\nu = 3$, with all heat being carried downstream by the integer $\nu = 1$ edge. Instead, we find a behaviour similar to what was observed at 8.3 T, with heating both upstream and downstream and a slight asymmetry between the two. This surprising result can be understood if we allow for the presence of additional structure in the $\nu = 1$ edge that does not affect charge transport. Perhaps the simplest such structure would be the presence of an incompressible strip of $\nu = 2/3$, much like what we see at 8.3 T, but with charge equilibrating between the two separated edges of this strip (Fig. 2III). With these edges equilibrated, we

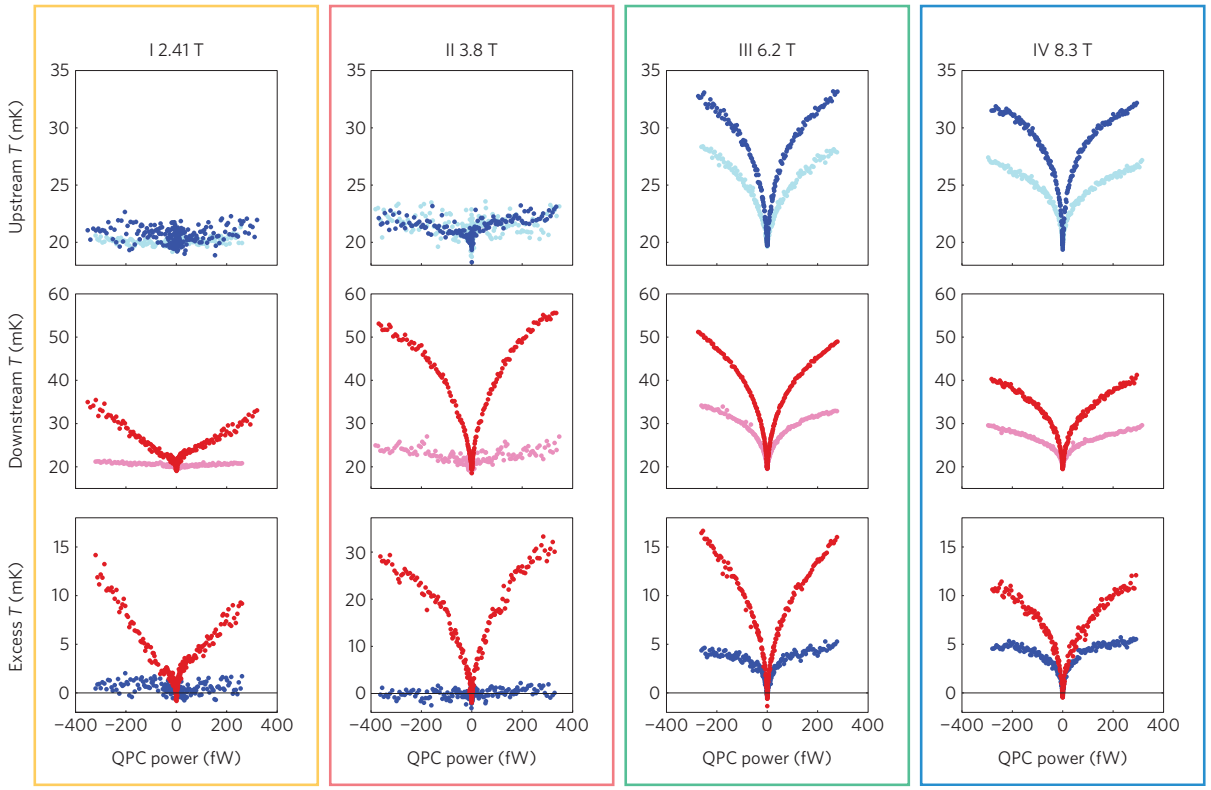

Figure 3 | Local edge temperature versus QPC power dissipation at different magnetic fields. Negative (positive) QPC powers correspond to the injection of holes (electrons). For each magnetic field, the upstream and downstream temperatures were measured with (blue, red) and without (cyan, magenta) the deflector gates energized. The difference between temperatures with and without the deflectors energized is plotted across the bottom row for the downstream (red) and upstream (blue) dots. For I and II, corresponding to an integer outermost edge, heat is carried chirally downstream with no upstream heat transport. For IV, where we measure a 2/3 outermost edge, the heat is carried downstream and upstream. For III, heat is also carried in both directions, while $R_L = 1$. We attribute this behaviour to reconstruction outside the bulk $\nu = 1$ edge, which allows upstream heat transport without 2/3 charge transport.

measure a local Hall resistance of $R_L = h/e^2$. However, the diffusive heat transport provided by the outer $\nu = 2/3 \rightarrow 0$ edge could still carry heat to the upstream thermometer (edge IV in Fig. 4). Importantly, this mechanism of upstream heating by an apparent $\nu = 1$ edge would not be universal and would depend sensitively on the spatial reconstruction of the edge. A sharper mesa-defined edge with a larger density gradient[14,21] or a lower-mobility 2DES may not allow an incompressible strip of $\nu = 2/3$ to form outside the $\nu = 1$ bulk. To clarify this, we will now consider a device with a mesa-defined edge.

Sharp confinement modifies edge structure

Here, we will present data from a sample in which we physically removed material to define the boundary of the 2DES, creating a steeper confining potential when compared with the device in Fig. 1. As a result of the steeper confinement, we find edges of type III and (IV; from Fig. 4) when the bulk is at $\nu = 1$. The gate-defined edge, as a reminder, had edges of type IV and V at bulk filling $\nu = 1$. From the table in Fig. 4, we see that charge transport (R_{xy} and R_L) cannot discriminate between the type III and type IV edges. We will now present evidence that both of these edges can exist in a single sample, and that they can be distinguished by monitoring upstream heat transport.

In Fig. 5, we present a scanning electron micrograph of the device under consideration. The device geometry and substrate used are identical to those used for the device presented in Fig. 1. Instead of using deflector gates to define the edge, we used a chemical etch to remove material between the QPC heater and the quantum dot thermometer. This creates a physical boundary to the sample along which the edge propagates. The density in the 2DES must drop to zero across this edge, which can happen over a shorter length scale than for an edge created by depleting the 2DES through electrostatic gating.

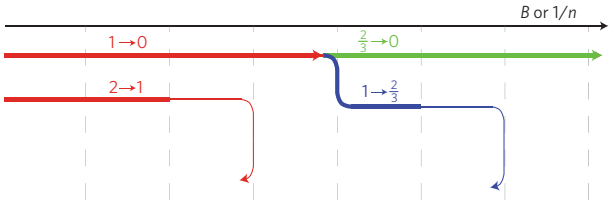

	I	II	III	IV	V	VI
R_{xy}^{-1}	2	2	1	1	1	2/3
R_L^{-1}	2	1	1	1	2/3	2/3
Upstream heat	No	No	No	Yes	Yes	Yes

Figure 4 | Possible edge structures at different magnetic fields. The width (and existence) of each given region will depend on details of the sample and the sharpness of the edge. Three types of edge are present in this experiment, denoted by different colours, with the topmost edge being the outer edge. Only edge structures II, IV and V are present in the device in Fig. 1. Edge III is present in the device in Fig. 5. All resistances are given in units of h/e^2. A measurement of R_{xy} allows one to determine the total conductance of all edges. A measurement of R_L allows one to determine which edges chemically equilibrate when charge is injected into the outer edge (denoted by bold lines in the figure). Only the $(2/3) \rightarrow 0$ edge transports heat upstream, and can be identified by thermometry measurements. Detecting upstream heat allows us to discriminate between edges III and IV.

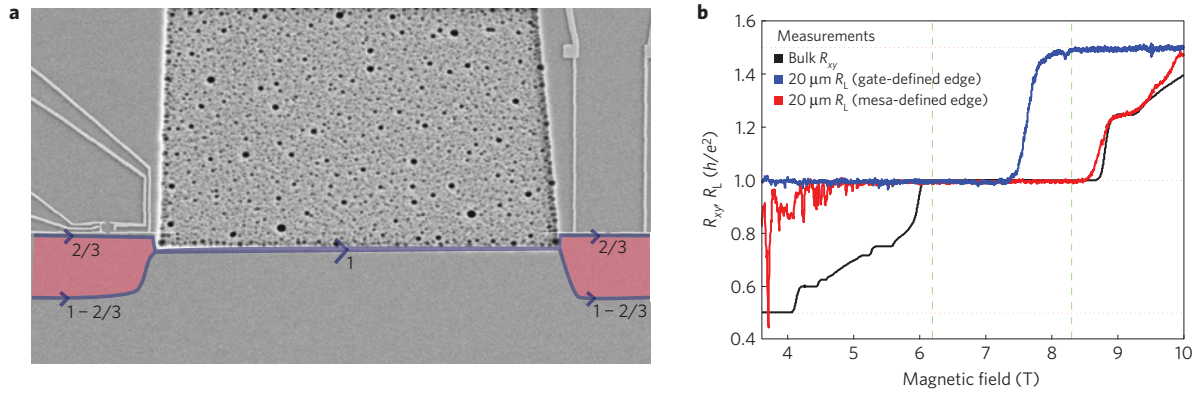

Figure 5 | Modified device to study heat transport along a sharper edge. The gate-defined edge (Fig. 1) allowed for a $\nu = 2/3$ edge to form outside the $\nu = 1$ bulk (blue trace in **b**). The mesa-defined edge here is sharper, and the sharp density gradient may preclude FQH edge structure outside the $\nu = 1$ bulk. **a**, Scanning electron micrograph of a device with 40 μm between the heater and the thermometer. The device measured had 20 μm between the heater and the thermometer, to match the device presented in Fig. 1. **b**, R_L (red) for the device in **a**. The reduced resistance of the edge (red versus blue) at 8.3 T when switching from a gate-defined to a mesa-defined edge suggests that the originally separated FQH ($\nu = 2/3$ and $\nu = 1 \rightarrow 2/3$) channels are brought close together, allowing charge to equilibrate between them. Although the device is drawn with an edge of type III (from Fig. 4), an edge of type IV cannot be ruled out from charge transport, either locally (R_L) or globally (R_{xy}). Dotted red lines indicate quantized values of R_L. Dashed green lines indicate fields at which thermometry measurements were made.

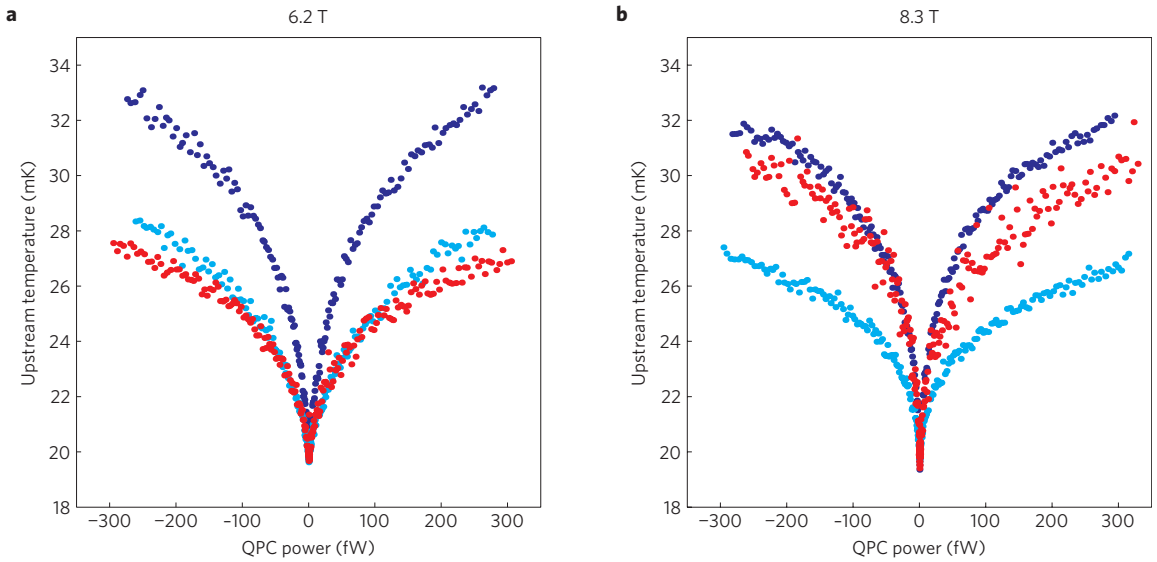

Figure 6 | Upstream thermometry to identify FQH structure in the $\nu = 1$ edge. Light blue curves depict background upstream heating, which we attribute to the bulk. The dark blue curves depict the heat observed with a gate-defined edge connecting the heater and the thermometer. The red curves depict upstream heat observed with a sharper mesa-defined edge connecting the heater and the thermometer. **a**, At low fields, the upstream heating from the mesa-defined edge closely matches the background, suggesting no excess heat is carried by the edge. **b**, At high fields, there is a similar amount of upstream heating by both sharp and shallow edges, both appreciably above the background.

To demonstrate that this edge is sharper, we can repeat our local charge transport measurements (Fig. 5b, R_L in red). The observed enhanced conductance at any given field (red compared with blue) is a result of either more edges participating in transport, or a greater conductance of participating edges. This is precisely what is expected if the edges are confined with a steeper potential. Here we will focus on behaviour on the edge of the $\nu = 1$ bulk (6.2 and 8.3 T). From the charge transport measurements, we cannot distinguish the exact edge structure at either field (see edges III and IV) in Fig. 4).

To distinguish between these two possible edge structures, we can perform upstream thermometry measurements. As we created our edge in this sample by etching the mesa, we cannot control for bulk heating by energizing and de-energizing deflection gates. However, by using an identical geometry to the gate-defined device, we can still identify the presence or absence of excess heat due to the edge. This thermometry measurement is presented in Fig. 6, with data from the edge-defined device in red. For comparison, data from the gate-defined device taken at the same fields are reproduced in dark blue and light blue (identical to upstream data in columns III and IV of Fig. 3).

At 6.2 T, we see that the temperature detected upstream (red in Fig. 6a) closely matches the temperature associated with bulk heating in the original device (light blue). This is consistent with no heat being transported by the edge. The lack of upstream heat carried by the edge allows us to classify it as a simple IQH $\nu = 1$ edge (type III in Fig. 4), similar to what was observed at bulk fillings of $\nu = 2$ and $\nu = 3$ in the original device.

At 8.3 T, the temperature measured upstream (red in Fig. 6b) seems to be elevated, closely matching the temperature seen when

a $\nu = 2/3$ edge connects the heater to the upstream thermometer in the original device (dark blue). Recall that in the original device, this $\nu = 2/3$ edge was detectable through measurement of R_L (blue curve in Fig. 2). Here the charge signature has vanished ($R_L = R_{xy}$), but the nearly identical upstream heating strongly suggests that the $\nu = 2/3$ edge is still present (edge IV in Fig. 4). These measurements increase our confidence in assigning edge IV to our observations at 6.2 T in the original device.

By studying the charge and heat transport properties of the outermost component of a gate-defined quantum Hall edge, these measurements suggest that such edges contain considerable structure. Charge transport along the edge shows that correlated FQH modes can exist outside an IQH bulk. Even when these charge signatures are not present (Fig. 2III and edge IV in Fig. 4), heat transport suggests that density reconstructions can still create edge components that carry heat upstream. The presence of such edge structure could have strong implications for the behaviour of quantum Hall interferometers, where integer edges are conventionally treated as featureless electron beams[23].

In addition to this, by separating bulk and edge contributions, we have been able to observe bulk heat transport at $\nu = 1$ that is absent at $\nu = 2$ and $\nu = 3$, the origin of which remains an open question.

More generally, our system provides a framework to extract quantitative information about charge and heat transport at the boundary of any 2D topological insulator. Such a system can be essential to discriminate between topological states of matter that have identical charge transport behaviour. For example, with the $\nu = 5/2$ FQH state, the presence or absence of these neutral modes would allow us to discriminate between distinct ground states that are particle–hole conjugates of each other[24–26].

Received 30 March 2012; accepted 5 July 2012; published online 5 August 2012

References

1. Girvin, S. & Prange, R. *The Quantum Hall Effect* (Springer, 1987).
2. Stern, A. & Halperin, B. I. Proposed experiments to probe the non-Abelian $\nu = 5/2$ quantum Hall state. *Phys. Rev. Lett.* **96,** 016802 (2006).
3. Bonderson, P., Kitaev, A. & Shtengel, K. Detecting non-abelian statistics in the $\nu = 5/2$ fractional quantum Hall state. *Phys. Rev. Lett.* **96,** 016803 (2006).
4. Chklovskii, D. B., Shklovskii, B. I. & Glazman, L. I. Electrostatics of edge channels. *Phys. Rev. B* **46,** 4026–4034 (1992).
5. Zhitenev, N. B., Haug, R. J., Klitzing, K. V. & Eberl, K. Time-resolved measurements of transport in edge channels. *Phys. Rev. Lett.* **71,** 2292–2295 (1993).
6. Hwang, S. W., Tsui, D. C. & Shayegan, M. Experimental evidence for finite-width edge channels in integer and fractional quantum Hall effects. *Phys. Rev. B* **48,** 8161–8165 (1993).
7. Yacoby, A., Hess, H., Fulton, T., Pfeiffer, L. & West, K. Electrical imaging of the quantum Hall state. *Solid State Commun.* **111,** 1–13 (1999).
8. Huber, M. *et al.* Structure of a single sharp quantum Hall edge probed by momentum-resolved tunneling. *Phys. Rev. Lett.* **94,** 016805 (2005).
9. MacDonald, A. H. Edge states in the fractional-quantum-Hall-effect regime. *Phys. Rev. Lett.* **64,** 220–223 (1990).
10. Wen, X. G. Electrodynamical properties of gapless edge excitations in the fractional quantum Hall states. *Phys. Rev. Lett.* **64,** 2206–2209 (1990).
11. Ashoori, R. C., Stormer, H. L., Pfeiffer, L. N., Baldwin, K. W. & West, K. Edge magnetoplasmons in the time domain. *Phys. Rev. B* **45,** 3894–3897 (1992).
12. Kane, C. L., Fisher, M. P. A. & Polchinski, J. Randomness at the edge: Theory of quantum Hall transport at filling $\nu = 2/3$. *Phys. Rev. Lett.* **72,** 4129–4132 (1994).
13. Kane, C. L. & Fisher, M. P. A. Quantized thermal transport in the fractional quantum Hall effect. *Phys. Rev. B* **55,** 15832–15837 (1997).
14. Bid, A. *et al.* Observation of neutral modes in the fractional quantum Hall regime. *Nature* **466,** 585–590 (2010).
15. Deviatov, E. V., Lorke, A., Biasiol, G. & Sorba, L. Energy transport by neutral collective excitations at the quantum Hall edge. *Phys. Rev. Lett.* **106,** 256802 (2011).
16. van Wees, B. J. *et al.* Anomalous integer quantum Hall effect in the ballistic regime with quantum point contacts. *Phys. Rev. Lett.* **62,** 1181–1184 (1989).
17. Kouwenhoven, L. P. *et al.* Selective population and detection of edge channels in the fractional quantum Hall regime. *Phys. Rev. Lett.* **64,** 685–688 (1990).
18. Altimiras, C. *et al.* Non-equilibrium edge-channel spectroscopy in the integer quantum Hall regime. *Nature Physics* **6,** 34–39 (2009).
19. Altimiras, C. *et al.* Tuning energy relaxation along quantum Hall channels. *Phys. Rev. Lett.* **105,** 226804 (2010).
20. Takei, S., Milletarì, M. & Rosenow, B. Nonequilibrium electron spectroscopy of Luttinger liquids. *Phys. Rev. B* **82,** 041306 (2010).
21. Granger, G., Eisenstein, J. P. & Reno, J. L. Observation of chiral heat transport in the quantum Hall regime. *Phys. Rev. Lett.* **102,** 086803 (2009).
22. Altimiras, C. *et al.* Chargeless heat transport in the fractional quantum Hall regime. *Phys. Rev. Lett.* **109,** 026803 (2012).
23. Deviatov, E. V., Ganczarczyk, A., Lorke, A., Biasiol, G. & Sorba, L. Quantum Hall Mach–Zehnder interferometer far beyond equilibrium. *Phys. Rev. B* **84,** 235313 (2011).
24. Lee, S.-S., Ryu, S., Nayak, C. & Fisher, M. P. A. Particle–hole symmetry and the $\nu = \frac{5}{2}$ quantum Hall state. *Phys. Rev. Lett.* **99,** 236807 (2007).
25. Levin, M., Halperin, B. I. & Rosenow, B. Particle-hole symmetry and the Pfaffian state. *Phys. Rev. Lett.* **99,** 236806 (2007).
26. Dolev, M. *et al.* Characterizing neutral modes of fractional states in the second Landau level. *Phys. Rev. Lett.* **107,** 036805 (2011).

Acknowledgements

We acknowledge financial support from Microsoft Corporation Project Q, the NSF GRFP and the DOE SCGF Program.

Author contributions

V.V. and S.H. conceived and designed the experiments, prepared samples, carried out the experiments and data analysis and wrote the paper. A.Y. conceived and designed the experiments, carried out data analysis and wrote the paper. L.N.P. and K.W.W. carried out the molecular beam epitaxy growth.

Additional information

Supplementary information is available in the online version of the paper. Reprints and permissions information is available online at www.nature.com/reprints. Correspondence and requests for materials should be addressed to A.Y.

Competing financial interests

The authors declare no competing financial interests.